Ultralow dose CT image reconstruction with pre-log shifted-Poisson model and texture-based MRF prior

Yuxiang Xing
Dept. of Engineering Physics
Tsinghua University
Beijing 100084, China
xingyx@mail.tsinghua.edu.cn

Hao Zhang
Biomedical Engineering Dept
Johns Hopkins University
Baltimore, MD 21205, USA

Junyan Rong, Hongbin Lu
Dept. of Biomedical Engineering
Fourth Military Medical University
Xi'an 710032, China

Zhengrong Liang
Depts. of Radiology and Biomedical Engineering
Stony Brook University
Long Island, NY 11794, USA

***Abstract*—Computed tomography (CT) dosage is a big concern in clinic. Low-dose CT has attracted a lot of attention in this field. Lowering dose leads to difficulties in reconstruction because of high noise level. In this work we study an ultralow dose CT by using a pre-log shifted-Poisson statistical model and proposed an iterative reconstruction method by optimizing an objective function consisted of pre-log shifted Poisson likelihood and a texture-based MRF (Markov random field). The proposed method was tested on a numerical phantom with ultralow incident photons and electronic noise, as well as an artificial ultralow data simulated from a high-dose patient data. Our results demonstrated the good performance gained from the pre-log shifted Poisson model and texture-based MRF prior.**

Keywords—Ultralow dose CT; pre-log shifted Poisson; image reconstruction; texture; MRF

I. INTRODUCTION

X-ray computed tomography (CT) is a widely-used imaging modality in clinic. Researchers have worked for decades to minimize the radiation-associated risk by both hardware and software innovations. In the software aspect, statistical modeling for an accurate cost function and iteratively minimizing the cost function for a smooth convergence toward an optimal reconstruction has shown promising performance in maintaining the image quality as compared to the traditional filtered back-projection (FBP) reconstruction while at much lower dose level. To gain more solid benefits from the statistical image modeling (SIM) reconstruction methods under the Bayesian theory, two key components are the research focuses: (1) the statistical properties of noise in the acquired data and (2) an appropriate *a priori* model for the to-be-reconstructed image.

Compound Poisson statistics for the X-ray counts and Gaussian distribution for the electronic background noise are commonly used to model the statistical properties of the data which lead to an intractable likelihood term in the Bayesian framework [1-4]. As a way around (or to circumvent) the intractable problem, an approximation is usually made by replacing the compound Poisson with the Poisson and further replacing the summation of the Poisson and Gaussian distributions as a shift Poisson distribution [5-6].

In the past decades, tremendous amount of work has been done on the *a priori* modeling of the to-be-reconstructed image in a concerned application. The *a priori* image modeling is frequently referred as regularization or penalty in the SIM reconstruction methods. General applicable non-linear priors such as Huber are proposed to preserve edges while de-noising at the same time [7-8]. More recently, efforts have been devoted to incorporating information from source such as the images from previous full-dose or diagnostic CT scan [9-12] and complete data sets [13-14].

In this work, we combined a tractable shifted Poisson model [15] for data statistics with our texture-based Markov random field (MRF) prior extracted from previous full-dose CT scans [12] to gain full power of SIM reconstruction for ultra-low dose CT imaging.

II. METHOD

In this work, we denote acquired data from a polychromatic X-ray CT system as a vector $\mathbf{I} \in \Re^{M\times 1}$, where M is the number of data elements. The effective attenuation map of an object is denoted by a vector $\boldsymbol{\mu} \in \Re^{N\times 1}$ with N being the dimension of lexicographically ordered pixels. With X-ray incident flux (together with detector efficiency) being $\{ I_i^0 \}$, where index i indicates the X-ray toward detector bin i, then the X-ray signals reaching a detector bin i can be expressed as $I_i^0 e^{-[\mathbf{A}\boldsymbol{\mu}]_i}$ in average sense (i.e. I_i^0 can be determined accurately by system calibration in the absence of body) according to Beer's law. Here, matrix $\mathbf{A}$ models the linear system relationship and is usually called projection matrix of size $M\times N$ with its element denoted by A_{mn}, and row vector denoted by $\mathbf{A}_m$. The acquired data include an additional Gaussian electronic noise, which we assume its mean $m_{e,i}$ and variance $\sigma_{e,i}^2$ predetermined at each detector bin i.

DOI: 10.12059/Fully3D.2017-11-3201012

A. *Texture-preserving Low-dose CT Image Reconstruction with Shifted-Poisson Data Model (SP-MRFt)*

Following the idea of [15], we set up an artificial random vector:

$$\mathbf{I}^{\mathrm{A}} \equiv \mathbf{I} - m_e + \sigma_e^2 \ . \tag{1}$$

where the mean m_e and variance σ_e^2 of the background noise are assumed to be the same for all detector bins for simplicity.

It can be easily shown that $\mathbf{I}^{\mathrm{A}}$ has its mean and variance both equal to $I_i^0 e^{-[\mathbf{A}\boldsymbol{\mu}]_i} + \sigma_e^2$. It was shown in [15] that $\left[\mathbf{I}^{\mathrm{A}}\right]_+$ could be very accurately described by a Poisson distribution. Therefore, we are able to get a tractable log-likelihood function for $\left[\mathbf{I}^{\mathrm{A}}\right]_+$:

$$L(\boldsymbol{\mu}) = \sum_m \left\{ I_m^{\mathrm{A}} \ln\left(I_m^0 \mathrm{e}^{-[\mathbf{A}\boldsymbol{\mu}]_m} + \sigma_e^2\right) - \left(I_m^0 \mathrm{e}^{-[\mathbf{A}\boldsymbol{\mu}]_m} + \sigma_e^2\right) \right\} \ . \tag{2}$$

It is necessary to enforce noise reduction in case of low dose high noise situation. As shown in [12], texture based MRF regularization can efficiently incorporating information from previous full-dose image and gain effective noise reduction with minimal cost of high-resolution details:

$$R(\boldsymbol{\mu}) = \frac{1}{2} \sum_{r=1}^{R} \sum_{n \in \mathrm{Rgn}(r)} \sum_{n' \in \Omega(n)} w_{nn'}^r (\mu_n - \mu_{n'})^2 \tag{3}$$

where, $\Omega(n)$ denotes neighborhood of pixel n and r indexes a region of certain tissue. Within each region, $w_{nn'}^r$ are shift-invariant MRF coefficients depending on neighboring relationship. Regions are segmented and classified based on different texture properties. These MRF coefficients are determined according to previous full-dose images under the principle of:

$$w_{nn'}^r = \arg\min \sum_{n \in \mathrm{Rgn}(r)} \sum_{n' \in \Omega(n)} (\mu_n^{\mathrm{FD}} - w_{nn'}^r \mu_{n'}^{\mathrm{FD}})^2 \quad \forall r \tag{4}$$

where, the superscript "FD" means full-dose. Eq. (4) is quadratic and a close form solution can be obtained.

$$\mathbf{w}^r = \left[\sum_{n \in \mathrm{Rgn}(r)} (\boldsymbol{\mu}_{\Omega_n}^{\mathrm{FD}} (\boldsymbol{\mu}_{\Omega_n}^{\mathrm{FD}})^T) \right]^{-1} \left[\sum_{n \in \mathrm{Rgn}(r)} (\boldsymbol{\mu}_{\Omega_n}^{\mathrm{FD}} \mu_n^{\mathrm{FD}}) \right] \tag{5}$$

where, we use $\boldsymbol{\mu}_{\Omega_n}^{\mathrm{FD}}$ to denote a lexicographically ordered neighboring pixels around pixel n for notation convenience, and $\mathbf{w}^r$ a corresponding vector of MRF coefficients for region r.

Combining (2) and (3) gives us an overall objective function to minimize in the framework of a Bayesian MAP image reconstruction:

$$\begin{aligned} \boldsymbol{\mu} &= \underset{\boldsymbol{\mu}}{\operatorname{argmin}} \Phi(\boldsymbol{\mu}) = \underset{\boldsymbol{\mu}}{\operatorname{argmin}} \left(-L(\boldsymbol{\mu}) + \beta R(\boldsymbol{\mu}) \right) \\ &= \underset{\boldsymbol{\mu}}{\operatorname{argmin}} \left\{ \begin{array}{l} \sum_m \left\{ \left(I_m^0 \mathrm{e}^{-[\mathbf{A}\boldsymbol{\mu}]_m} + \sigma_e^2 \right) - I_m^{\mathrm{A}} \ln\left(I_m^0 \mathrm{e}^{-[\mathbf{A}\boldsymbol{\mu}]_m} + \sigma_e^2 \right) \right\} \\ + \frac{\beta}{2} \sum_{r=1}^{R} \sum_{n \in \mathrm{Region}(r)} \sum_{n' \in \Omega(n)} w_{nn'}^r (\mu_n - \mu_{n'})^2 \end{array} \right\} \end{aligned} \tag{6}$$

where β is a parameter of balancing the data fidelity term of (2) and the priori term of (3).

B. *Implementation Algorithm for the Presented Reconstruction Method*

From the theory in last subsection, we can see that the objective function is composed of a non-quadratic part and a quadratic part. The situation of low-dose data acquisition even makes the condition of the non-quadratic part worse (i.e. very small condition number). Also, it is a non-separable function of huge number of unknown variables $\boldsymbol{\mu}$. In response, we derive its separable surrogate function based on [16].

In (2), for each ray path, we denote a function $h_m(l_m)$: $h_m(l_m) = (I_m^0 \mathrm{e}^{-l_m} + \sigma_e^2) - I_m^{\mathrm{A}} \ln(I_m^0 \mathrm{e}^{-l_m} + \sigma_e^2)$ with its 1st derivative being: $h_m'(l_m^k) = I_m^0 \mathrm{e}^{-l_m^k} \left(\frac{I_m^A}{I_m^0 \mathrm{e}^{-l_m^k} + \sigma_e^2} - 1 \right)$.

In the k^{th} iteration, a global surrogate function for the likelihood term in (6) would be:

$$\begin{aligned} \phi(\boldsymbol{\mu}; \boldsymbol{\mu}^k) &= \sum_m h_m(l_m^k) + \sum_m h_m'(l_m^k)(l - l_m^k) + \frac{1}{2} \sum_m c_m(l_m^k)(l - l_m^k)^2 \\ &= \sum_m h_m\left(\left[\mathbf{A}\boldsymbol{\mu}^k \right]_m \right) + \sum_m h_m'\left(\left[\mathbf{A}\boldsymbol{\mu}^k \right]_m \right) \left([\mathbf{A}\boldsymbol{\mu}]_m - \left[\mathbf{A}\boldsymbol{\mu}^k \right]_m \right) \\ &\quad + \frac{1}{2} \sum_m c_m\left(\left[\mathbf{A}\boldsymbol{\mu}^k \right]_m \right) \left([\mathbf{A}\boldsymbol{\mu}]_m - \left[\mathbf{A}\boldsymbol{\mu}^k \right]_m \right)^2 \end{aligned} \tag{7}$$

where, $\boldsymbol{\mu}^k$ denote the current estimation, c_m is chosen to ensure monotonic decreasing:

$$c_m\left(l_m^k\right) = \begin{cases} \left[\frac{2}{(l_m^k)^2} \left(\begin{array}{l} I_m^0 \left(1 - \mathrm{e}^{-l_m^k}\right) - I_m^{\mathrm{A}} \log \frac{I_m^0 + \sigma_e^2}{I_m^0 \mathrm{e}^{-l_m^k} + \sigma_e^2} \\ + l_m^k I_m^0 \mathrm{e}^{-l_m^k} \left(\frac{I_m^{\mathrm{A}}}{I_m^0 \mathrm{e}^{-l_m^k} + \sigma_e^2} - 1 \right) \end{array} \right) \right]_+ & l_m^k > 0 \\ \left[I_m^0 \left(1 - \frac{I_m^{\mathrm{A}} \sigma_e^2}{\left(I_m^0 + \sigma_e^2 \right)^2} \right) \right]_+ & \text{else} \end{cases}$$

Because the function for each ray is quadratic, i.e. convex, (7) can be further relaxed to a separable function by using convexity property with the trick that:

$$[\mathbf{A}\boldsymbol{\mu}]_m = \sum_n A_{mn} \mu_n = \sum_n \alpha_{mn} \left[\frac{A_{mn}}{\alpha_{mn}} (\mu_n - \mu_n^k) + l_m^k \right] \ .$$

By choosing $\alpha_{mn} = \frac{A_{mn}}{|\mathbf{A}_m|}$, $|\mathbf{A}_m| = \sum_n A_{mn}$, we can get:

$$-L\left(\boldsymbol{\mu};\boldsymbol{\mu}^k\right) \le \sum_n \sum_m \frac{A_{mn}}{|\mathbf{A}_m|} \left\{ \begin{array}{l} h(l_m^k) + h_m^{'}(l_m^k)\left(|\mathbf{A}_m|(\mu_n - \mu_n^k)\right) \\ +\frac{1}{2} c_i(l_m^k)\left(|\mathbf{A}_m|(\mu_n - \mu_n^k)\right)^2 \end{array} \right\} \quad (8)$$

For the regularization term $R(\boldsymbol{\mu})$, because it is quadratic, we can gain a separable surrogate function using the trick:

$$(\mu_n - \mu_{n'})^2 \le \frac{1}{2}\left(2\mu_n - \mu_n^k - \mu_{n'}^k\right)^2 + \frac{1}{2}\left(2\mu_{n'} - \mu_n^k - \mu_{n'}^k\right)^2,$$

so that

$$\begin{aligned} R(\boldsymbol{\mu}) &\le \frac{1}{4}\sum_{r=1}^{R} \sum_{n\in \mathrm{Rgn}(r)} \sum_{n'\in\Omega(n)} w_{nn'}^r \left((2\mu_n - \mu_n^k - \mu_{n'}^k)^2 + (2\mu_{n'} - \mu_n^k - \mu_{n'}^k)^2\right) \\ &= \frac{1}{2}\sum_{r=1}^{R} \sum_{n\in \mathrm{Rgn}(r)} \sum_{n'\in\Omega(n)} w_{nn'}^r (2\mu_n - \mu_n^k - \mu_{n'}^k)^2 \end{aligned} \quad (9)$$

Eqs. (8) and (9) together gives us an overall separable surrogate function:

$$\begin{aligned} \Phi\left(\boldsymbol{\mu};\boldsymbol{\mu}^k\right) = \sum_n \sum_m \frac{A_{mn}}{|\mathbf{A}_m|} \left\{ \begin{array}{l} h(l_m^k) + h_m^{'}(l_m^k)\left(|\mathbf{A}_m|(\mu_n - \mu_n^k)\right) \\ +\frac{1}{2} c_i(l_m^k)\left(|\mathbf{A}_m|(\mu_n - \mu_n^k)\right)^2 \end{array} \right\} \\ + \frac{\beta}{2}\sum_{r=1}^{R} \sum_{n\in \mathrm{Rgn}(r)} \sum_{n'\in\Omega(n)} w_{nn'}^r (2\mu_n - \mu_n^k - \mu_{n'}^k)^2 \end{aligned} \quad (10)$$

According Newton's algorithm, we can get a parallelizable update formula for our ultralow-dose image reconstruction method:

$$\mu_n^{k+1} = \mu_n^k - \left\{ \frac{\partial^2 \Phi\left(\boldsymbol{\mu};\boldsymbol{\mu}^k\right)}{\partial \mu_n^{\,2}} \right\}\Bigg|_{\mu_n^k}^{-1} \frac{\partial \Phi\left(\boldsymbol{\mu};\boldsymbol{\mu}^k\right)}{\partial \mu_n}\Bigg|_{\mu_n^k} \quad (11)$$

with

$$\begin{aligned} \frac{\partial \Phi\left(\boldsymbol{\mu};\boldsymbol{\mu}^k\right)}{\partial \mu_n}\Bigg|_{\mu_n^k} &= \sum_m A_{mn} I_m^0 \mathrm{e}^{-l_m^k}\left(\frac{I_m^{\mathrm{A}}}{I_m^0 \mathrm{e}^{-l_m^k} + \sigma_e^2} - 1\right) \\ &+ \beta \sum_{n'\in\Omega(n)} (w_{nn'} + w_{n'n})\left(\mu_n^k - \mu_{n'}^k\right) \end{aligned} \quad (12)$$

$$\left\{ \frac{\partial^2 \Phi\left(\boldsymbol{\mu};\boldsymbol{\mu}^k\right)}{\partial \mu_n^2} \right\}\Bigg|_{\mu_n^k} = \sum_m A_{mn} c_m\left(l_m^k\right)|\mathbf{A}_m| + 2\beta \sum_{n'\in\Omega(n)} (w_{nn'} + w_{n'n}) \quad (13)$$

The implementation of the above SP-MRFt algorithm representation can be summarized by the following pseudo code:

a) Segment $\boldsymbol{\mu}$ from the full dose image into 4 classes.
b) Estimate MRF coefficient $w_{nn'}^r$ for each class according to the full dose image [12].
c) Initialize image by the FBP reconstruction from the ultralow-dose data;
d) While stop criterion is not met:
   i. Update μ_n using Eq. (11-13) with β =0.
   End if stop criterion is satisfied.
e) Segment the resulted $\hat{\boldsymbol{\mu}}$ in step (d) into four classes of tissues.
f) Assign $w_{nn'}^r$ to each pixel according to its class.
g) While stop criterion is not met:
   i. Update μ_n using Eq. (11-13) with a certain β;
   End if stop criterion is satisfied.

III. Experimental Results

We validated our reconstruction method on patient ultra-low dose (ULD) CT data with both numerical simulation and artificial ULD data based on real data. In numerical simulation, we modeled a case with 2000 incident photons and standard deviation = 30 for electronic noise. A chest 2D phantom from NCAT as shown in Fig. 1 was used with materials defined in Table I.

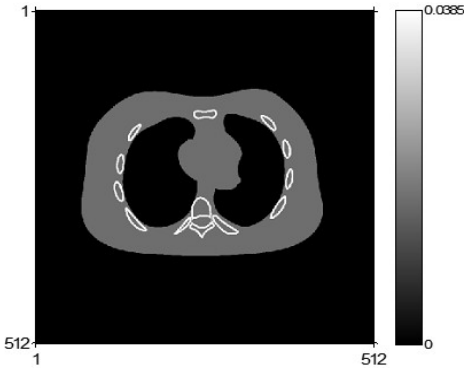

Fig. 1 numerical NCAT chest phantom.

Table I matters in numerical chest phantom

tissue	linear attenuation coef. (1/mm)
lung	$2.00*10^{-5}$
fat	$1.66*10^{-2}$
Spine and Rib	$3.85*10^{-2}$
spinal marrow	$1.66*10^{-2}$

Fig. 2 shows the reconstruction results with FBP, post-log weighted least squares (WLS), and pre-log shifted Poisson model without prior. It's obvious that the pre-log shifted Poisson can significantly reduce the streaking artifacts caused by photon starvation in the ULD case. We also produced an ULD CT data based on a real full-dose (100 mA) patient data but using 5mA electrical current level with electronic noise of standard deviation = 20 added. Reconstruction results from FBP with full-dose data and ULD data, as well as the pre-log shifted Poisson, and SP-MRFt are compared in Fig. 3. In the SP-MRFt implementation, MRF coefficients for lung, bone, fat and muscle are computed from FBP reconstruction of the full-dose data (shown in Fig. 4). The hyper-parameter β for the prior was set to be 5000. In such an ULD case, FBP reconstruction is of really poor image quality. With the pre-

log shifted Poisson model, most of the structures in the object can be reconstructed though not as good as the full-dose FBP. Furthermore, with the texture-based MRF prior, noise in different tissues can be rather properly restrained.

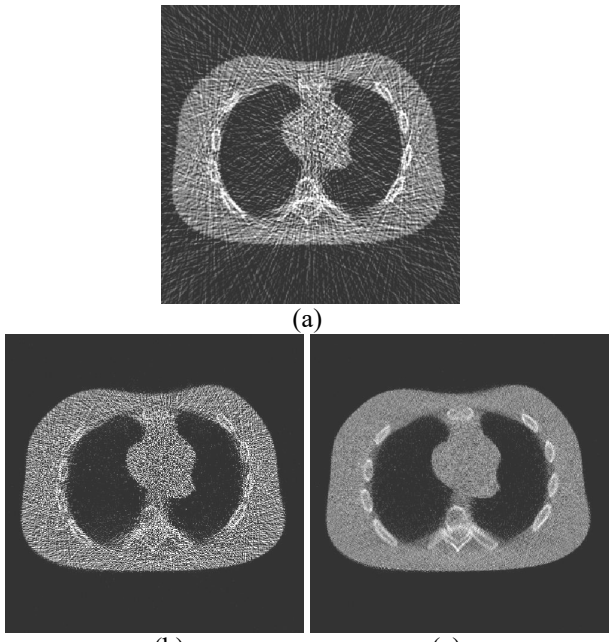

Fig. 2 Reconstruction results with different models for the NCAT chest phantom in the case of ultralow-dose. (a) FBP, (b) post-log WLS, and (c) pre-log shifted Poisson.

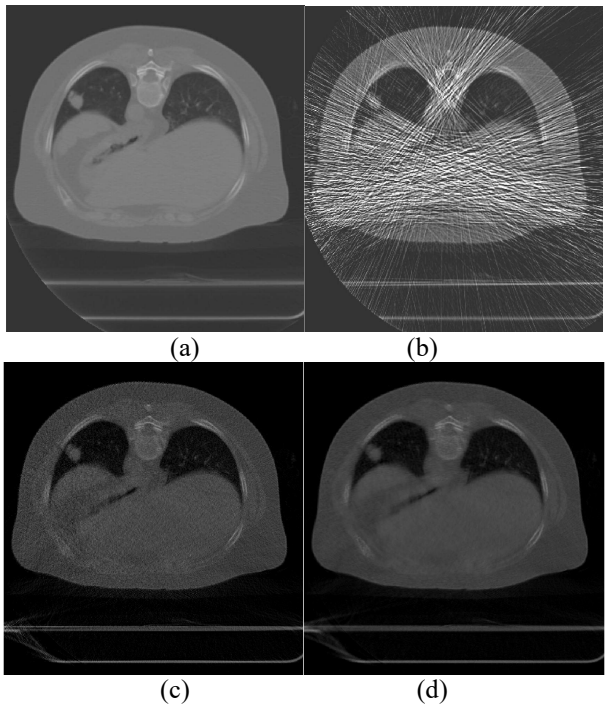

Fig. 3. Reconstruction results with different methods. From left to right: full dose FBP, ultralow dose FBP, ultralow dose with pre-log shifted Poisson, ultralow-dose with pre-log shifted Poisson and texture prior (β=10000).

IV. Conclusion and Discussion

Ultralow-dose CT imaging has been a desired task with a lot of attention in the field. The artifacts of ultralow-dose images are mainly caused by the rays of very weak signals. In this work, we present an iterative reconstruction method based on the pre-log shifted Poisson statistical model together with a texture-based MRF prior constraint for ultralow-dose CT imaging. Experimental studies show that the pre-log shifted Poisson model can well characterize the rays with photon starvation problem and give rather good reconstructions. Moreover, it can easily combine the texture-based prior to further reduce noise-induced artifacts with little lose in resolution. Further investigation is under progress.

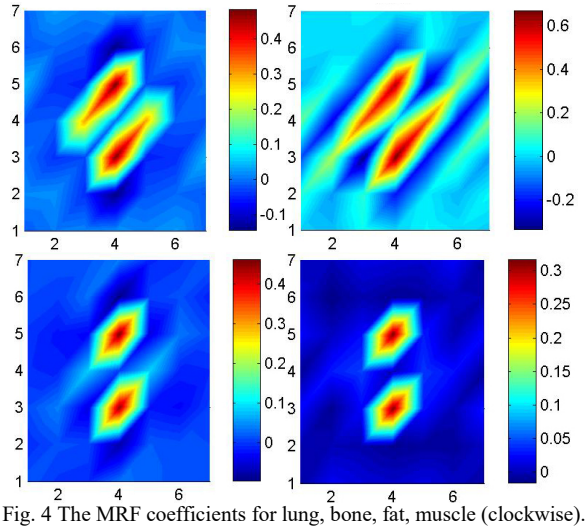

Fig. 4 The MRF coefficients for lung, bone, fat, muscle (clockwise).

Acknowledgment

Dr. Xing was partially supported by NNSFC #11275104, Dr. Liang was partially supported by the National Institutes of Health under grants #CA206171 and #CA143111, Dr. Rong was partially supported by the Natural Nature Science Foundation of Shaanxi Province under grant #2016JQ1012 and Dr. Lu was partially supported by NNSFC #81230035.

References

[1] B R Whiting, S Kingshighway, and S L Mo, “Signal statistics of X-ray Computed Tomography,” Proc. SPIE Medical Imaging, 2002, 4682: 53–60.

[2] I A Elbakri and J A Fessler, “Efficient and accurate likelihood for iterative image reconstruction in x-ray computed tomography,” Proc. SPIE Medical Imaging, 2003, 5032: 1839–1850.

[3] G M Lasio, B R Whiting, and J F Williamson. "Statistical reconstruction for x-ray computed tomography using energy-integrating detectors," Physics in Medicine and Biology, 2007, 52(8): 2247.

[4] J Wang, H Lu, Z Liang, D Eremina, G Zhang, S Wang, J Chen, and J Manzione, “An Experimental Study on the Noise Properties of X-ray CT Sinogram Data in Radon Space,” Physics in Medicine and Biology, 2008, 53(12): 3327–3341.

[5] D L Snyder, C W Helstrom, and A D Lanterman, “Compensation for readout noise in CCD images,” Journal of Optical Society of America A, 1995, 12(2): 272–283.

[6] P J Rivière, “Penalized-likelihood sinogram smoothing for low-dose CT,” Medical Physics, 2005, 32(6): 1676–1683.

[7] J Wang, T Li, and L Xing. "Iterative image reconstruction for CBCT using edge-preserving prior," Medical physics, 2009, 36(1): 252–260.

[8] K J Little and P J Rivière, “Sinogram restoration in computed tomography with an edge-preserving penalty,” Medical Physics, 2015, 42: 1307–1320.

[9] B Nett, J Tang, B Aagaard-Kienitz, H Rowley, and G Chen, “Low radiation dose C-arm cone-beam CT based on prior image constrained compressed sensing (PICCS): Including compensation for image volume mismatch between multiple data acquisitions,” Proc. SPIE Medical Imaging, 2009, 7258: 725–803.

[10] J Ma, J Huang, Q Feng, H Zhang, H Lu, Z Liang, and W Chen, “Low-dose CT image restoration using previous normal-dose scan,” Medical Physics, 2011, 38: 5713–5731.

[11] L Ouyang, T Solberg, and J Wang, “Noise reduction in low-dose cone beam CT by incorporating prior volumetric image information,” Medical Physics, 2012, 39: 2569–2577.

[12] H Zhang, H Han, Z Liang, Y Hu, Y Liu, W Moore, J Ma, and H Lu, “Extracting information from previous full-dose CT scan for knowledge-based Bayesian reconstruction of current low-dose CT images,” IEEE Transactions on Medical Imaging, 2016, 35(3): 860–70.

[13] G Chen, J Tang, and S Leng, "Prior image constrained compressed sensing (PICCS): A method to accurately reconstruct dynamic CT images from highly under-sampled projection data sets," Medical Physics, 2008, 35: 660–663.

[14] L Shen and Y Xing. "Multi-energy CT acquisition and reconstruction with a stepped tube potential scan," Medical Physics, 2015, 42(1): 282–296.

[15] M Yavuz and J A Fessler. "Statistical image reconstruction methods for randoms-precorrected PET scans," Medical Image Analysis, 1998, 2(4): 369–378.

[16] H Erdogan and J A Fessler. "Monotonic algorithms for transmission tomography," The 5th IEEE EMBS International Summer School, Biomedical Imaging, 2002.